CHALMERS
UNIVERSITY OF TECHNOLOGY

Unsteady 3-D RANS simulations of dust explosion in a fan stirred explosion vessel using an open source code

Journal of Loss Prevention in the Process Industries 67 (2020) 104237

Contents lists available at ScienceDirect

Journal of Loss Prevention in the Process Industries

journal homepage: http://www.elsevier.com/locate/jlp

Unsteady 3-D RANS simulations of dust explosion in a fan stirred explosion vessel using an open source code

Chen Huang [a,*], Andrei N. Lipatnikov [b], Ken Nessvi [c]

[a] Department of Safety and Transport, RISE Research Institutes of Sweden, Box 857, SE-501 15, Borås, Sweden
[b] Department of Mechanics and Maritime Sciences, Chalmers University of Technology, SE-412 96, Göteborg, Sweden
[c] BSL Industri, Grynbodgatan 3, SE-211 33, Malmö, Sweden

ARTICLE INFO

Keywords:
Dust explosion
Computational Fluid Dynamics
Premixed turbulent combustion
Open source
OpenFOAM
Modelling

ABSTRACT

Dust explosion is a constant threat to industries which deal with combustible powders such as woodworking, metal processing, food and feed, pharmaceuticals and additive industries. The current standards regarding dust explosion venting protecting systems, such as EN 14491 (2012) and NFPA 68 (2018), are based on empirical correlations and neglect effects due to complex geometry. Such a simplification may lead to failure in estimating explosion overpressure, thus, increasing risk for injuries and even fatalities at workplaces. Therefore, there is a strong need for a numerical tool for designing explosion protecting systems. This work aims at contributing to the development of such a tool by (i) implementing a premixed turbulent combustion model into OpenFOAM, (ii) verifying the implementation using benchmark analytical solutions, and (iii) validating the numerical platform against experimental data on cornflour dust explosion in a fan-stirred explosion vessel, obtained by Bradley et al. (1989a) under well-controlled laboratory conditions.

For this purpose, the so-called Flame Speed Closure model of the influence of turbulence on premixed combustion is adapted and implemented into OpenFOAM. The implementation of the model is verified using exact and approximate analytical solutions for statistically one-dimensional planar and spherical turbulent flames, respectively. The developed numerical platform is applied to unsteady three-dimensional Reynolds Averaged Navier-Stokes simulations of the aforementioned experiments. The results show that the major trends, i.e. (i) a linear increase in an apparent turbulent flame speed $S_{t,b}$ with an increase in the root mean square (rms) turbulent velocity u' and (ii) and an increase in $S_{t,b}$ with an increase in the mean flame radius, are qualitatively predicted. Furthermore, the measured and computed dependencies of $S_{t,b}(u')$ agree quantitatively under conditions of weak and moderate turbulence.

1. Introduction

Dust explosion is a constant threat to industries which deal with combustible solids, e.g. woodworking, metal processing, food and feed, pharmaceuticals and additive industries. A dust explosion can occur if the concentration of dust-air cloud is within flammability limits and there is an energy supply sufficient for igniting the mixture. Statistics shows that there is one serious dust explosion every day in Europe alone (Beck and Jeske, 1982).

To manage the dust explosion risk, a proper risk assessment must be carried out. As a basis of the risk assessment, one have to establish the explosion characteristics of the dust, which involve Minimum Explosive Concentration (MEC), deflagration index K_{St}, maximum explosion overpressure P_{max}, Minimum Ignition Energy (MIE), Minimum Ignition Temperature (MIT), etc. These data are then used to assess the likelihood and the consequences of an explosion. Subsequently, risk evaluation is performed by comparing results of the risk assessment with established risk criteria in order to determine whether additional protection measures are required. Such measures can be of both organisational and technical nature. The organisational measures involve training the staff to raise awareness of the explosion hazards, proper housekeeping, maintenance, procedures for hot work permit, etc. The technical measures include, e.g., installation of dust extraction systems to limit explosive atmospheres, the use of a proper ATEX-approved equipment in explosive atmospheres to avoid ignition, or installation of explosion protection systems such as venting, suppression, isolation, and

* Corresponding author. Box 857, SE-501 15, Borås, Sweden.
E-mail address: chen.huang@ri.se (C. Huang).

https://doi.org/10.1016/j.jlp.2020.104237
Received 8 May 2020; Received in revised form 3 July 2020; Accepted 14 July 2020
Available online 24 July 2020
0950-4230/

containment.

The consequences of a dust explosion are highly dependent on the explosion development, i.e., the rate of the explosion pressure rise, the maximum explosion pressure, the flame propagation speed, etc. Accordingly, the explosion development depends on dust characteristics, operating conditions (pressure, flow rate, turbulence level, initial temperature), geometry of the equipment (scale, interconnection of vessels, congestion, etc.), as well as the location of ignition point and the strength of the ignition source. Consequently, assessing the explosion severity is a huge challenge, especially in facilities with complex processes and geometries. Therefore, there is a great need for new tools to improve predicting explosion patterns. Development of Computational Fluid Dynamics (CFD) tools is a promising approach to meet this request.

The advantages of CFD tools are as follows. First, they can be used to design explosion protecting systems for process plants with complicated geometries where the current standards, e.g. EN14491 (2012), VDI3673 (2002) and NFPA68 (2018), are not applicable. Second, many virtual experiments can be performed using CFD tools, thus, saving a lot of money for avoiding expensive large-scale experiments. Third, physics-based dust explosion models and numerical tools can be used to improve the current standards regarding explosion protection design.

Open Field Operation and Manipulation (OpenFOAM, 2019) software is a suitable platform for developing efficient CFD tools for research into dust explosions. It is a free, open-source general-purpose CFD software package mainly for simulating thermodynamics, fluid dynamics, and chemical reactions. On the technical side, OpenFOAM excels in modern architecture using object-orientated programming language, high parallelization and unstructured grid for dealing with curved geometry. New models and methods can be implemented and tested thanks to the open source. Furthermore, OpenFOAM creates more value for a customer, because it offers an opportunity to create a tailor-made tool that suits the special need of the customer at zero license cost. At the same time, the cost of personal hours in using OpenFOAM may be higher when compared to a commercial CFD code, which benefits from detailed documentation, training, and dedicated technical support. It is also worth noting that OpenFOAM is distributed under version 3 of the GNU General Public License (GPLv3), which gives the users a great freedom in adapting it. For example, users are free (i) to use OpenFOAM for both commercial and non-commercial purposes, (ii) to change the code, (iii) to share the code, and (iv) to share the changes they made. However, this freedom may have negative consequences, e.g., the code developments often suffer from the lack of the detailed documentation readily available to the community.

OpenFOAM was already applied to simulating gas explosions. For instance, Bauwens et al. (2008) studied methane-air deflagration in a vented enclosure experimentally and numerically within the framework of Large Eddy Simulation (LES). Encouraging agreement in terms of explosion overpressure and flame velocities were obtained between experiments and simulations. Later, Bauwens et al. (2011) modelled vented explosion of lean hydrogen-air mixtures by taking into consideration the Darrieus-Landau and Rayleigh-Taylor instabilities.

Based on OpenFOAM, Vendra and Wen (2019) developed a CFD tool for LES of vented deflagration of lean hydrogen-air mixtures. The combustion model used by them is based on (i) a default premixed turbulent combustion model in OpenFOAM (Weller et al., 1998) and (ii) a model of the Darrieus-Landau and Rayleigh-Taylor instabilities, proposed by Bauwens et al. (2011). Sinha et al. (2019) also used the above-mentioned tool for the same application.

Examples of comprehensive benchmark studies on vented hydrogen explosions were reported by Tolias et al. (2018), Vyazmina et al. (2019), and Skjold et al. (2019a, 2019b). The scatter of their results, e.g. explosion overpressure yielded by different CFD tools, calls for more research in this area.

As far as dust explosions are concerned, Spijker et al. (2013) modelled lycopodium dust explosion in a tube using a modified solver in OpenFOAM. More often, dust explosions are computed using other numerical tools.

In particular, within the framework of a European Union project called DESC (Dust Explosion Simulation Code), researchers developed the DESC code, which later became a submodule in a commercial CFD software FLACS distributed by Gexcon for simulating gas and dust explosions (Skjold, 2007). The dust explosion module, i.e. FLACS-DustEx, has been developed by comparing simulation results with data measured in various experiments of different scales (Skjold, 2003, 2007; Skjold et al., 2005, 2006). The FLACS-DustEx flame propagation model addresses fine dust particles with high volatile contents (Skjold, 2014) and, accordingly, is based on a model used earlier for gas-air explosions. Tascón and Aguado (2015) applied FLACS-DustEx to study dust explosions in industrial scenarios and reported satisfactory agreement between computed results and experimental data or dust explosion venting standards. However, certain problems need to be resolved to improve the model and code, e.g. (i) the use of a single-block structured mesh, which yields over-prediction of momentum dissipation over sloping area (Gant and Hoyes, 2010), (ii) the lack of choice of different turbulence models when compared to a general-purpose CFD software, and (iii) grid-dependence problem associated with combustion model (Skjold, 2014; Tascón and Aguado, 2017).

Besides commercial software, inhouse code were also developed by several research groups for studying gas and dust explosions. For example, Ugarte et al. (2016) and Sezer et al. (2017) simulated vented gas explosions using a phenomenological model and a single-zone approximation. Demir et al. (2017, 2018) modelled gas and dust explosions in coal mines by studying two flame acceleration mechanisms and compressibility effects. Moreover, numerical studies of induced layered dust explosions were performed by Song et al. (2017), Song and Zhang (2019), and Shimura and Matsuo (2019), but codes used in those studies are not discussed in the cited papers.

Furthermore, hydrogen explosion with suspended inert dust particles were studied by Liberman et al. (2015) in the framework of Direct Numerical Simulation (DNS). However, DNS technique is not realistic for solving engineering problems due to its extremely high computational cost.

Thus, gas and dust explosions are computed adopting various numerical tools that range from (i) engineering models (e.g. FLACS-DustEx), which can be used at industrial scales, but invoke oversimplified phenomenological models of ignition and turbulent combustion, to (ii) detailed models that allow for basic physical phenomena at relatively small spatial scales, but are not yet feasible for simulations at industrial scales. Accordingly, a comparison between the different types of models is not straightforward. Nevertheless, due to rapid development of computer hardware, there is clear trend towards applications of detailed models to problems characterized by larger scales. In line with this trend, there is a growing interest in applying efficient and well-validated detailed models of turbulent combustion to safety problems.

In particular, under certain conditions, the dust explosion process resembles turbulent burning of a gas cloud. This is especially true for very fine organic dust particles with high volatile content (Bradley et al., 1988, 1989a; 1989b). Therefore, a premixed turbulent combustion model is sometimes used for CFD modelling of dust explosions (Spijker et al., 2013; Skjold, 2014). The present work aims at adapting the so-called Flame Speed Closure (FSC) model of the influence of turbulence on premixed burning (Lipatnikov and Chomiak, 1997, 2002a) for this purpose. The main reason is that, as reviewed elsewhere (Lipatnikov and Chomiak, 2002a; Lipatnikov, 2012, 2018), the FSC model has been quantitatively validated against a wide set of experimental data obtained by various research groups from various (both expanding and statistically stationary) flames under a wide range of substantially different conditions (various fuels, equivalence ratios, initial temperatures, pressures, rms turbulent velocities, and turbulent length scales). Moreover, the FSC model is an extension of the well-known Turbulent Flame Closure (TFC) model (Zimont and Lipatnikov, 1993, 1995; Karpov

et al., 1996), which has been implemented into various commercial CFD codes, e.g., Ansys CFX (Ansys, 2020a), Ansys Fluent (Ansys, 2020b), Converge (2020), FINE (FINE, 2019), AVL FIRE (AVL FIRE, 2020). Accordingly, the TFC model is widely used by automotive and gas turbine industry.

More specifically, this work aims at (i) implementing the FSC model into the open source toolbox OpenFOAM, (ii) verifying the model implementation using exact and approximate analytical solutions for statistically 1-D, planar and spherical, respectively, premixed flames expanding in "frozen" turbulence, and (iii) validating the developed numerical platform against experimental data obtained by Bradley et al. (1989a) utilizing the well-known Leeds fan stirred explosion vessel.

In the next section, the FSC model is briefly summarized. Numerical and experimental setups adopted for verification of the model implementation and for validation of the numerical platform are described in Sect. 3. Computed results are discussed in Sect. 4, followed by conclusions.

2. FSC model

2.1. Model equations

The FSC model (i) characterizes the thermochemical state of a reacting mixture in a flame using a single combustion progress variable c, which is equal to zero and unity in fresh reactants and equilibrium combustion products, respectively, (ii) invokes the following well-known Bray-Moss-Libby (BML) equations (Bray and Moss, 1977; Libby and Bray, 1977)

$$\overline{\rho} = \frac{\rho_u}{1+(\sigma-1)\tilde{c}}, \qquad \overline{\rho c} = \rho_b \overline{c}, \tag{1}$$

and (iii) deals with the following transport equation

$$\frac{\partial \overline{\rho}\tilde{c}}{\partial t} + \nabla\cdot(\overline{\rho}\tilde{\mathbf{u}}\tilde{c}) = \nabla\cdot[\overline{\rho}(\kappa + D_t)\nabla\tilde{c}] + \rho_u U_t|\nabla\tilde{c}| + Q, \tag{2}$$

for the Favre-averaged combustion progress variable $\tilde{c}$. Here, ρ is the density; $\sigma = \rho_u/\rho_b$ is the density ratio; t is the time; $\mathbf{u}$ is the flow velocity vector; κ is the molecular heat diffusivity of the mixture; D_t and U_t are the turbulent diffusivity and burning velocity, respectively; Q is a source term discussed later, see Eq. (6); over-lines designate the Reynolds average, while $\tilde{q} = \overline{\rho q}/\overline{\rho}$ is the Favre-averaged value of q with $q'' = q - \tilde{q}$; subscripts u and b designate unburned and burned gas, respectively.

Within the framework of the FSC model, D_t and U_t are evaluated as follows (Lipatnikov and Chomiak, 1997, 2002a)

$$D_t = D_{t,\infty}\left[1 - \exp\left(-\frac{t_{fd}}{\tau_L}\right)\right], \tag{3}$$

$$U_t = U_{t,ISP}\left[1 - \frac{\tau_L}{t_{fd}} + \frac{\tau_L}{t_{fd}}\exp\left(-\frac{t_{fd}}{\tau_L}\right)\right]^{1/2}, \tag{4}$$

where $D_{t,\infty}$ is the fully developed turbulent diffusivity, which can be determined using a turbulence model, as will be discussed later; t_{fd} is the flame development time counted starting from end of ignition; $\tau_L = D_{t,\infty}/u'^2$ is the Lagrangian time scale of turbulence; u' is the rms turbulent velocity;

$$U_{t,ISP} = A u' Da^{1/4} \tag{5}$$

is an intermediately steady turbulent burning velocity; $A = 0.4$ (Lipatnikov and Chomiak, 1997) is the sole constant of the FSC model; $Da = \tau_t/\tau_f$ is the Damköhler number; $\tau_t = L/u'$ and $\tau_f = \delta_L/S_L$ are turbulent and laminar-flame time scales, respectively; L is an integral turbulent length scale; S_L and $\delta_L = \kappa_u/S_L$ are the laminar flame speed and thickness, respectively. As discussed in detail elsewhere (Zimont, 1979; Lipatnikov and Chomiak, 2002a; Lipatnikov, 2012), at moderate turbulence, Eq. (5) is qualitatively consistent with various experimental data on the influence of mixture composition, turbulence characteristics, and pressure on turbulent burning velocity or flame speed.

Originally, Eq. (5) was analytically derived by Zimont (1979) by assuming that (i) small-scale eddies increase local burning velocity by thickening flamelets and increasing heat and mass transfer within them, with the width of the thickened flamelets being still significantly smaller than L; (ii) large-scale eddies increase local burning velocity by wrinkling the thickened flamelets; and (iii) the mean turbulent flame brush thickness δ_t grows by the turbulent diffusion law. Such a regime characterized by apparently stationary turbulent burning velocity given by Eq. (5), but growing δ_t was later called Intermediate Steady Propagation (ISP) regime (Zimont, 2000). Numerous experimental data reviewed elsewhere (Prudnikov, 1967; Lipatnikov and Chomiak, 2002a) indicate that such a combustion regime is a widespread regime of premixed turbulent burning.

The original derivation of Eq. (5) was performed under the following constraints: the turbulent Reynolds number $Re_t = u'L/\nu_u \gg 1$, $Da \gg 1$, the Karlovitz number $Ka = Re_t^{1/2}/Da > 1$, and $\tau_t < t_{fd} \ll \tau_t Da^{1/2}$ (Zimont, 1979). Here, ν_u is the kinematic viscosity of unburned gas. Subsequently, Lipatnikov and Chomiak (2002a) argued that the aforementioned assumption (i), i.e. thickening of flamelets by small-scale eddies, could be substituted with a more general assumption that the interaction between small-scale turbulent eddies and flamelets is controlled by the mean dissipation rate $\tilde{\varepsilon}$ and chemical time scale τ_c. Under this assumption, which is in fact an extension of the well-recognized Kolmogorov hypothesis to the case of premixed turbulent combustion, the constraint of $Ka > 1$ is substituted with $u'/S_L > 1$ and the model is applicable to moderately turbulent burning also.

If $D_t = D_{t,\infty}$, $U_t = U_{t,ISP}$, and $Q = 0$ in Eq. (2), the FSC model reduces to the TFC model by Zimont and Lipatnikov (1993, 1995). The time-dependent terms in square brackets in Eqs. (3) and (4) extend the TFC model and allow us to simulate early stages of premixed turbulent flame development, including the formation of a small flame kernel after ignition, transition to turbulent burning, and development of the turbulent flame. Equation (3) is well known in the turbulence literature (Hinze, 1975) and results from the Taylor (1935) theory of turbulent diffusion. Equation (4) was derived by Lipatnikov and Chomiak (1997) by adapting the Taylor's theory to extend the Zimont model of the intermediately steady turbulent burning velocity.

In order to (i) simulate an early stage of flame kernel growth after spark ignition and (ii) obtain an appropriate balance equation in the limit case of $u' \to 0$, the TFC model was further extended and the following source term (Lipatnikov and Chomiak, 1997, 2002a)

$$Q = \frac{\overline{\rho}(1-\tilde{c})}{t_r(1 + D_t/\kappa_b)}\exp\left(-\frac{\Theta}{\tilde{T}}\right) \tag{6}$$

was incorporated into in Eq. (2). Here, Θ is the activation temperature for a single reaction that the combustion chemistry is reduced to ($\Theta = 20000$ K in the present work); the Favre-averaged temperature $\tilde{T}$ is evaluated using the simplest form $\overline{\rho}\tilde{T} = \rho_u T_u$ of the ideal gas state equation; and the reaction time scale t_r is set so that, in the case of $u' = 0$, the burning velocity yielded by stationary, 1-D Eqs. (1), (2) and (6) is equal to the laminar burning velocity S_L, which is an input parameter of the model. This constraint results in

$$t_r = \Psi^2\left(\frac{T_b}{T_u}, \frac{\Theta}{T_u}\right)\frac{\kappa_u}{S_L^2}, \tag{7}$$

where the non-dimensional function Ψ approximates values of $S_L\sqrt{t_r/\kappa_u}$, pre-computed for various ratios of T_b/T_u and Θ/T_u by numerically integrating 1-D Eqs. (1), (2) and (6) with $D_t = U_t = 0$. In this case, the FSC Eq. (2) reduces to an equation that models a laminar premixed flame in the case of a single combustion reaction, with the source term Q being introduced into Eq. (2) by Lipatnikov and Chomiak (1997, 2002a) in

order to satisfy this constraint. A polynomial approximation of the function Ψ does not feature any tuning parameter and is reported by Huang et al. (2016).

2.2. Basic features

If $Q = 0$ in Eq. (2), there is the following exact analytical travelling-wave solution (Lipatnikov and Chomiak, 2005a, 2005b; Lipatnikov, 2009)

$$\overline{c} = \frac{1}{2} erfc\left(\xi\sqrt{\pi}\right) = \frac{1}{\sqrt{\pi}} \int_{\xi\sqrt{\pi}}^{\infty} e^{-\zeta^2} d\zeta, \tag{8}$$

$$\xi = \frac{x - x_f(t)}{\delta_t(t)}, \tag{9}$$

$$x_f(t) = x_f(t=0) + \int_0^t U_t(\theta) d\theta, \tag{10}$$

and

$$\delta_t^2(t) = 4\pi \int_0^t D_t(\theta) d\theta \tag{11}$$

to Eqs. (1)–(4) for a statistically 1-D planar flame that propagates from left to right.

Equations (8) and (9) describe a flame with a self-similar mean structure. As reviewed elsewhere (Prudnikov, 1967; Lipatnikov and Chomiak, 2002a; Driscoll, 2008; Lipatnikov, 2018) and supported by more recent experimental data (Tamadonfar and Gülder, 2014; Han et al., 2018), various premixed turbulent flames do have such a self-similar mean structure well described by Eqs. (8) and (9). It is worth stressing that a transport equation, which (i) was basically similar to Eq. (2), (ii) had the exact solution given by Eqs. (8)-(11), but (iii) was written in a different form, was introduced into the combustion literature by Prudnikov (1967) by considering statistically 1-D planar case.

Equation (11) predicts that the growth of $\delta_t(t)$ follows the turbulent diffusion law. Indeed, as hypothesized by Karlovitz et al. (1951), reviewed elsewhere (Prudnikov, 1967; Lipatnikov and Chomiak, 2002a; Driscoll, 2008; Lipatnikov, 2018) and supported by more recent data (Sponfeldner et al., 2015; Han et al., 2018), the growth of mean turbulent flame brush thickness does follow the turbulent diffusion law in various experiments.

In the statistically 1-D, but spherical case, the solution given by Eqs. (8)-(11) is not exact. Nevertheless, if the mean flame structure is assumed to be self-similar, i.e. $\overline{c}(r,t) = \overline{c}[(r - \overline{R}_f)/\delta_t]$ where r is the radial distance and $\overline{R}_f$ is a mean flame radius, the following analytical relation holds (Lipatnikov and Chomiak, 2007)

$$\frac{d\overline{R}_f}{dt} = \sigma U_t \left(\int_0^{\infty} \tilde{c} r dr \right) \left(\int_0^{\infty} \overline{c} r dr \right)^{-1} \tag{12}$$

for a particular mean flame radius defined elsewhere (Lipatnikov and Chomiak, 2002b), with this result agreeing quantitatively with the Leeds experimental data (Bradley et al., 2003).

Finally, as already noted in Sect. 1 and discussed in detail elsewhere (Lipatnikov and Chomiak, 2002a; Lipatnikov, 2012, 2018), the FSC model was quantitatively validated in RANS simulations of a wide set of experiments performed by various research groups with various (both expanding and statistically stationary) flames under a wide range of substantially different conditions (various fuels, equivalence ratios, initial temperatures, pressures, rms turbulent velocities, and turbulent length scales).

3. Numerical and experimental setups

Equations (1)–(7) were implemented into OpenFOAM, followed by application of the developed numerical platform to simulating experiments by Bradley et al. (1989a). In this section the numerical setups for verification of the model implementation is reported, followed by descriptions of the experimental and numerical setups for the Leeds fan-stirred explosion vessel.

3.1. Numerical setup for verification of model implementation

In order to directly verify the implementation of the FSC model into OpenFOAM, statistically 1-D, planar or spherical, premixed turbulent flames propagating in a statistically "frozen" turbulence characterized by stationary and spatially uniform u', L, and $D_{t,\infty}$ were simulated and computed results were compared with the exact or approximate, respectively, solution given by Eqs. (8)-(11) or (12), respectively. The simplification of statistically "frozen" turbulence was necessary at this stage of research, because the solutions were obtained in the case of spatially uniform u', L, and $D_{t,\infty}$. While the two benchmark problems are statistically 1-D, the RANS simulations were performed in 3-D cases.

Bearing in mind subsequent application of the FSC model to the dust explosion experiments, the simulation input parameters were set based on the experimental conditions. In particular, premixed burning of cornflour dust cloud was simulated. The cornflour chemical equivalent formula is $C_6H_{7.88}O_{4.98}$ with a heat of reaction being 15.8 MJ/kg (Bradley et al., 1989a). The corresponding single-step chemical mechanism is as follows

$$C_6H_{7.88}O_{4.98} + 5.48\ (O_2 + 3.71\ N_2) = 6CO_2 + 3.94H_2O + 20.331\ N_2$$

To verify the model implementation in the planar benchmark case, the computational domain is set to be a parallelepiped of a length of 0.1 m and a cross section of 0.003 × 0.003 m. The numerical mesh consists of 100 cells in the x direction and three cells in the y or z direction. The flame propagates from left to right. Zero velocity and free entrainment boundary conditions are set on the right (unburned) and the left (burned) boundaries, respectively.

To verify the model implementation in the spherical benchmark case, the computational domain is set to be a cube, which represents one eighth of the total volume filled with reactants or products. The cube side length is 60 mm and the mesh size is 0.25 mm in each direction. Totally 13 824 000 cells are created. The initial conditions correspond to a spherical kernel of a radius of 20 mm, filled with combustion products ($\tilde{c} = 1$). The rest of the domain is filled with unburned mixture ($\tilde{c} = 0$). Symmetry boundary conditions are set at three boundaries. Zero velocity and free entrainment boundary conditions are set at other three boundaries.

Other details are provided in Tables 1–3, where W is molecular weight, μ is the molecular dynamic viscosity of a mixture, $\tilde{k}$ is the Favre-averaged turbulent energy, and $\tilde{b} = 1 - \tilde{c}$ is the combustion regress

Table 1
Thermo-physical properties.

Parameters		Value
Unburned	T_u [K]	328
	W_u [g/mol]	32.8
	ρ_u [kg/m^3]	1.32
	μ_u [kg/(m·s)]	1.8e-5
Burned	T_b [K]	1500
	W_b [g/mol]	29.7
	ρ_b [kg/m^3]	0.248
	μ_b [kg/(m·s)]	4.6e-5
Flame	$\sigma = \rho_u/\rho_b = (T_b W_u)/(T_u W_b)$ [-]	5.06
	S_L [m/s]	0.12

Table 2
Initial conditions.

parameters	Value
T_0 [K]	328
P_0 [Pa]	11 000
$\tilde{k}$ [m^2/s^2]	0.96
u' [m/s]	0.8
$\tilde{\varepsilon}$ [m^2/s^3]	11.84, 69.6, 348
L [m]	0.029, 0.005, 0.001

Table 3
Boundary conditions in OpenFOAM.

	burned (left)	unburned (right)
P [Pa]	totalPressure	fixedValue 11 0000
$\tilde{\mathbf{u}}$ [m/s]	pressureInletOutletVelocity	fixedValue (0 0 0)
$\tilde{T}$ [K]	zeroGradient	fixedValue 328
$\tilde{b}$ [-]	zeroGradient	fixedvalue 1

variable.

3.2. Experimental setup for leeds fan stirred explosion vessel

The Leeds experiments (Bradley et al., 1989a) were performed by (i) filling a vessel with air and cornflour dust, (ii) mixing the dust and air by counter-rotating fans, which also generated statistically stationary homogeneous isotropic turbulence in the central part of the vessel, (iii) igniting the mixture by a spark located in the vessel centre, and (iv) recording images of expanding flames using high speed Schlieren technique. The vessel diameter is equal to 305 mm and its volume is about 0.023 m^3. The vessel has three pairs of orthogonal quartz windows of 150 mm diameter for optical measurements.

Turbulence was generated by four fans, whose rotation speed was changed to vary the rms turbulent velocity u'. In the discussed experiments, the fan speed was varied from 8 to 50 Hz, which corresponded to variations in u' from 0.80 to 5.0 m/s. While the integral length scale was not reported by Bradley et al. (1989a), it was reported in other papers by the Leeds group. In particular, Bradley et al. (2003) stated that the longitudinal integral length scale measured using laser Doppler velocimetry was found "*to be* 20 mm *and independent of fan speed between 1000 and 10* 000 rpm", with 1000 rpm corresponding to 16.5 Hz. It is worth noting, however, that, in the experiments with the lean dust-air mixture, the lowest fan speed was less than 16.5 Hz and a decrease in L at low fan speeds was reported in an earlier paper by the Leeds group (Abdel-Gayed et al., 1984). However, those data cannot be used here, because they were obtained using thermo-anemometry, but such a method performs poorly in flows with zero mean velocity. For instance, the earlier Leeds measurements with thermo-anemometry overestimated L at large fan speeds by a factor of about two. Thus, in the Leeds experiments with the dust-air mixture, the turbulence length scale of 20 mm could be overestimated at low fan speeds. Nevertheless, when compared to other experimental data on dust explosions, the Leeds measurements were performed under well-defined laboratory conditions, i.e. the initial and boundary conditions were controlled sufficiently well.

To study dust explosion, a premixed dust-air cloud was ignited by a spark in turbulent medium in the centre of the vessel. Subsequently, turbulent flame kernel growth was recorded using high-speed Schlieren system. By processing Schlieren images, an equivalent mean flame radius $\overline{R}_f$, i.e. the radius of a circle whose area was equal to the area enveloped by the flame surface on the image, was calculated and turbulent flame speed with respect to combustion products was evaluated by differentiating the measured $\overline{R}_f(t)$-curves, i.e.

$$S_{t,b} = \frac{d\overline{R}_f}{dt}. \tag{13}$$

To mitigate an influence of the spark on the flame speed, the measurements were performed in a range of 20 mm$\leq \overline{R}_f(t) \leq$35 mm. For such flame kernels, whose radius was less than the vessel radius by a factor of more than four, an increase in the pressure in the vessel was negligible.

In addition to the values of $S_{t,b}$ obtained at four different $\overline{R}_f$ and five different fan speeds, Bradley et al. (1989a) also reported the values of the laminar flame speed S_L and density ratio σ for the studied dust-air mixture. However, methods and precision of evaluation of these quantities are not discussed in the cited paper. Furthermore, the value of the laminar flame thickness δ_L, which is required to calculate an important input parameter of the FSC mode such as the chemical time scale $\tau_c = \delta_L/S_L$, is not reported either. Thus, even in the considered case of the small-scale well-controlled Leeds experiments, some information important for the model validation is missing. This is a typical problem for testing any model of dust explosion.

In this regard, it is worth noting that one of the biggest challenges associated with dust explosion modelling consists of a limited amount of data on the laminar flame speed. Unlike gas explosions, where S_L is a well-studied basic characteristic, the laminar flame speed of a dust-air cloud is rarely available. This parameter depends not only on the dust concentration, but also the dust particle size distribution and moisture content. Indeed, Cloney et al. (2018) studied the laminar flame propagation in a dust-air cloud using a detailed CFD model in OpenFOAM. The model took into account surface reactions, devolitization, and gas phase reactions. The reported results indicate substantial effects of the particle size distribution and initial temperature on the computed S_L. A method for modelling the effect of the particle size distribution on the speed of a laminar dust-air flame was recently proposed by Ghaffari et al. (2019). Fortunately, Bradley et al. (1989a) reported the value of S_L for the conditions of their experiments and this value is used in the present study.

3.3. Simulations of dust explosion in the Leeds fan stirred explosion vessel

To save computational time, one eighth of a cube whose volume is equal to the volume of the vessel is simulated, as sketched in Fig. 1. Accordingly, the length of the computational domain is 0.14 m. A grading method is used to generate the computational mesh with a finer mesh of about 0.125 mm in the centre and coarser mesh of about 3.6 mm in the far-field. The total mesh consists of 2 197 000 cells. A single simulation run takes around 2–4 days on two cores on a computer with 128 GB RAM and totally 28 Xeon Gold cores for a simulation duration of

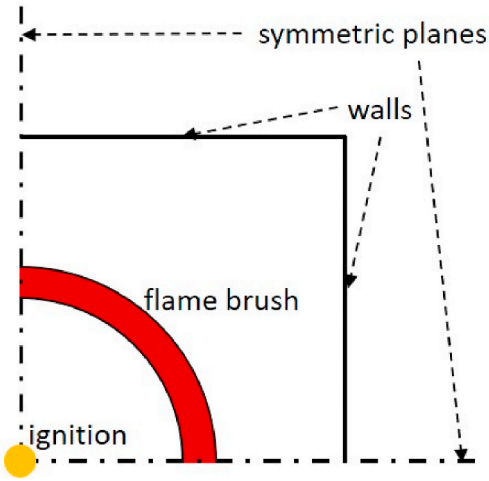

Fig. 1. Schematic illustration of cornflour dust explosion model.

30 ms using a maximum Courant number of 0.1. Grid sensitivity of numerical results was tested by varying the mesh in the centre from 0.0625 to 0.25 mm, with the computed dependencies of $S_{t,b}$ on $\overline{R}_f$ being close to one another.

The thermo-physical properties and boundary conditions are reported in Tables 1 and 3, respectively. It is worth noting that the measured burned temperature of 1500 K (Bradley et al., 1989a) is used here instead of the calculated burned temperature of 1592 K, because neither the method, nor precision of the calculation is discussed in the cited paper. The use of the former temperature yields the density ratio of 5.06, whereas $\sigma = 5.49$ reported by Bradley et al. (1989a) corresponds to the latter (higher) temperature.

To mimic spark ignition, the following extra source term

$$\overline{\rho}W_{ign} = \overline{\rho}W_0 \exp\left\{ -\left[\left(\frac{r}{\sigma_r}\right)^2 + H(t_0 - t)\left(\frac{t - t_0}{\sigma_t}\right)^2\right]\right\}(1 - \tilde{c}) \tag{14}$$

is added on the right hand side of Eq. (2). Here, $H(t_0 - t)$ is Heaviside function, while W_0, σ_r, σ_t are parameters of the ignition submodel. More specifically, t_0 is associated with ignition time, σ_t characterizes ignition duration, and σ_r corresponds to the size of ignition kernel. The factor W_0 is associated with the ignition strength and should be set sufficiently large in order for $\tilde{c}(r = 0, t_0)$ to be close to unity. A similar method was earlier used by Zimont and Lipatnikov (1993, 1995) and Karpov et al. (1996) to simulate experiments with flames expanding in a fan-stirred bomb, but the Heaviside function was skipped in the cited papers. The point is that if $Q = 0$ in Eq. (2), then, any $\tilde{c}(\mathbf{x},t) = \text{const}$ is a solution to it. Accordingly, due to numerical errors, $\tilde{c}(\mathbf{x}, t)$ tends often to zero in the entire computational domain. The use of the algebraic source term Q modelled with Eq. (6) resolves the problem (Lipatnikov and Chomiak, 1997), but provided that the magnitude of Q is sufficiently large. Under conditions of the present simulations, this is not so due to a low value of the laminar flame speed for the considered dust-air mixture. Therefore, to retain $\tilde{c}(r = 0, t > t_0) \approx 1$, the source term given by Eq. (14) is independent of time if $t > t_0$. Nevertheless, due to a low value of σ_r, the ignition source term is significant at small r only and weakly affects the speed $S_{t,b}$ of large flame kernels. For instance, $S_{t,b}$ computed at 20 mm$\leq \overline{R}_f(t) \leq$35 mm setting either $W_0 = 10^7$ s^{-1} and $\sigma_r = 0.5$ mm or $W_0 = 10^{13}$ s^{-1} and $\sigma_r = 0.25$ mm are very close to one another. Results reported in Sect. 4.2 were obtained using $\sigma_r = 0.25$ mm, $W_0 = 10^{13}$ s^{-1}, and $t_0 = 1$ ms.

To evaluate turbulence characteristics required by the FSC model, the following equations

$$D_{t,\infty} = \frac{C_\mu}{Pr_t}\frac{\tilde{k}^2}{\tilde{\varepsilon}}, \tag{15}$$

$$L = C_d\frac{\tilde{k}^{3/2}}{\tilde{\varepsilon}}, \tag{16}$$

$$\tilde{k} = \frac{3}{2}u'^2 \tag{17}$$

and the $k - \varepsilon$ turbulence model (Launder and Spalding, 1972) implemented into the standard OpenFOAM are used. Here, Pr_t is the turbulent Prandtl number, $C_\mu = 0.09$ is a constant of the $k - \varepsilon$ model, and $C_d = 1.0$. The turbulence model is switched on at $t \geq 2t_0$ to avoid unphysically strong generation of turbulence due to rapid density drop in the vessel centre, caused by the ignition source term W_{ign}. To mimic the flux of turbulent energy from the fans to the vessel centre and to simulate statistically stationary turbulence in line with the experiments, the extra source terms $\overline{\rho}\varepsilon_0$ and $\overline{\rho}\varepsilon_0^2/k_0$ are added on the right hand sides of the transport equations for $\tilde{k}$ and $\tilde{\varepsilon}$, respectively, following Zimont and Lipatnikov (1995). Here, k_0 and ε_0 are the initial values of the turbulent kinetic energy and its dissipation rate, respectively, reported in Table 4. Due to this modification, the values of u' and L upstream of the flame remain close to their initial values and are weakly affected by C_d.

Table 4
Initial turbulence characteristics.

u' [m/s]	0.80	1.62	2.45	3.31
k_0 [m^2/s^2]	0.96	3.94	9.00	16.43
ε_0[m^2/s^3]	47.03	390.53	1350.84	3331.12

4. Results and discussions

In this section, results of verification of the model implementation will be presented, followed by validation of the FSC model against the experimental data by Bradley et al. (1989a).

4.1. Verification of model implementation

Fig. 2a shows that the spatial profiles of the Reynolds-averaged combustion progress variable $\overline{c}$, simulated for the statistically 1-D planar flame, change with time. However, the same profiles plotted vs. the normalized distance ξ defined by Eq. (9) are almost the same at all time instants, see broken lines in Fig. 2b, in line with the well-documented self-similarity of premixed flames (Lipatnikov, 2009). Moreover, this computed self-similar profile agrees very well with the analytical solution given by Eq. (8), cf. solid and broken lines in Fig. 2b.

Comparison between calculated and analytical flame speeds is shown in Fig. 3. In the simulations, the flame speed is evaluated by taking derivative of the mean flame position against time. The mean flame position is defined by the x-coordinate of a surface of $\overline{c}(x, t) = 0.5$ (Lipatnikov and Chomiak, 2002b, 2007). Since the calculated flame speed exhibits fluctuations, UnivariateSpline function in scipy library of Python is used to smooth the data. Fig. 3 shows that the numerical and analytical results agree well. There is a slight discrepancy in the beginning of the simulations. This is caused by the usage of smoothing function in python.

Fig. 4 further verifies the implementation of the FSC model by showing that the mean flame brush thickness evaluated by processing the computed profiles of $\overline{c}(x, t)$ using the following equation

$$\delta_t(t) = \frac{1}{\max\{|\nabla\overline{c}|\}} \tag{18}$$

agrees very well with the analytical solution given by Eq. (11).

Fig. 5 shows that the spatial profiles of the Reynolds-averaged combustion progress variable $\overline{c}$, simulated for the statistically 1-D spherical flame, change with time but collapse to the same curve when plotted vs. the normalized distance ξ defined by Eq. (9), see broken lines in Fig. 5b, in line with the well-documented self-similarity of premixed flames. Moreover, this computed self-similar profile agrees well with the analytical solution given by Eq. (8), cf. solid and broken lines in Fig. 5b. It is worth remembering that both the self-similarity of the mean flame structure and Eq. (8) are well supported by experimental data obtained from various flame configurations and different (statistically stationary or expanding) types of flames (Lipatnikov and Chomiak, 2002a; Driscoll, 2008; Lipatnikov, 2012).

Fig. 6 shows that ratios of $\int_0^\infty \tilde{c}rdr\left\{\int_0^\infty \overline{c}rdr\right\}^{-1}$ and $S_{t,b}/(\sigma U_t)$, are sufficiently close to one another, in line with Eq. (12), thus, further verifying the model implementation. The two ratios are not exactly equal, because Eq. (12) is not exact.

4.2. Model validation

The discussed combination of the FSC model of the influence of turbulence on combustion and the $k - \varepsilon$ model of turbulence involves

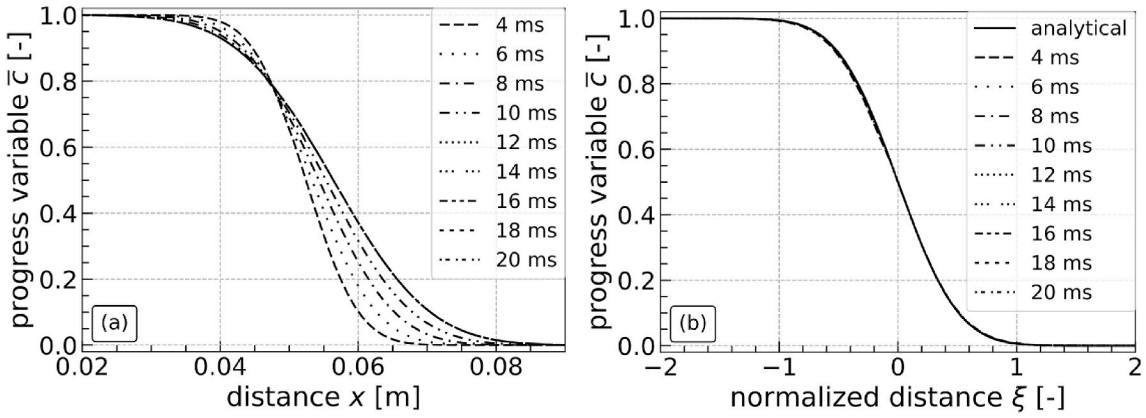

Fig. 2. Spatial profiles of the Reynolds-averaged combustion progress variable obtained from statistically 1-D planar flame propagating in "frozen" turbulence. (a) Reynolds-averaged combustion progress variable $\bar{c}$ vs. distance x, (b) $\bar{c}$ vs. the normalized distance ξ defined by Eq. (9).

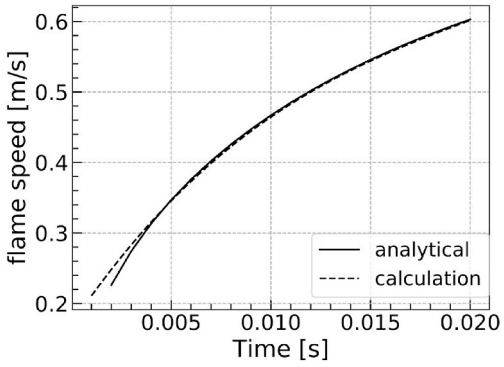

Fig. 3. Comparison of calculated flame speed with the flame speed given by Eq. (4) for statistically 1-D planar flame.

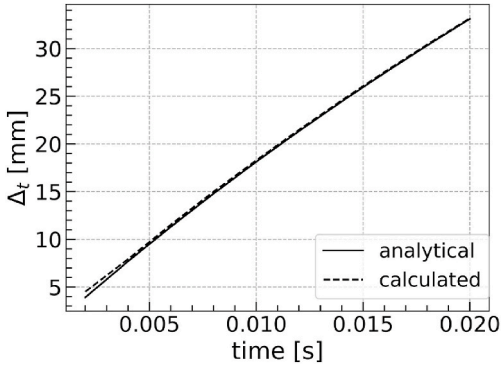

Fig. 4. Comparison of the mean flame brush thickness $\delta_t(t)$ calculated using Eq. (18) with the analytical solution given by Eq. (11).

two constants: the sole constant A of the FSC model, see Eq. (5), and the turbulent Prandtl number Pr_t required to evaluate turbulent diffusivity, see Eq. (15). In the present study, the standard value of $A = 0.4$ was used, but Pr_t was tuned to get the best agreement with the experimental data. Sensitivity of the computed results to Pr_t is illustrated in Fig. 7. In the literature, different values of Pr_t can be found, with Pr_t being varied between 0.3 and 1.0 when using Eq. (15) jointly with the TFC or FSC model (Lipatnikov, 2018). In the present study, the best agreement with the measured data is obtained for $Pr_t = 0.4$, which is sufficiently close to $Pr_t = 0.3$ recommended in recent papers (Yasari et al., 2015; Verma and Lipatnikov, 2016).

Results of the model validation are reported in Figs. 8 and 9. Here, the mean flame position is defined by the x-coordinate of a surface of $\bar{c}(x, t) = 0.1$, which differs from a value used to verify the model implementation. The reason is that $\bar{c}(x, t) = 0.1$ is associated with the high speed Schlieren technique used in the experiments, because this technique captures the leading edge of the mean flame brush, whereas Eq. (12) has been obtained for the radius of a surface of $\bar{c}(x, t) = 0.5$ (Lipatnikov and Chomiak, 2007). Comparison of open and filled symbols in Fig. 8 shows that the simulations well predict an increase in $S_{t,b}$ by u' in weak and moderate turbulence. Note that $S_{t,b}$ measured by Bradley et al. (1989a) at $u' = 5$ m/s is significantly less than at $u' = 3.31$ m/s. Such a decrease in flame speed by the rms turbulent velocity in intense turbulence is well documented in various experiments with flames expanding in a fan-stirred bomb since the seminal study by Karpov et al. (1959). However, available combustion models cannot predict this phenomenon without tuning, as discussed in detail elsewhere (Lipatnikov and Chomiak, 2002a, 2005c). For this reason, the present study is restricted to $u' \leq 3.31$ m/s.

It is of interest to note that Fig. 8 shows almost linear correlation between computed (or measured) flame speeds and rms turbulent velocity. For instance, for the mean flame radius of 30 mm, the computed results (open squares) are well fitted with the following linear equation

$$S_{t,b} = 0.6923\, u' + 0.4727. \tag{19}$$

On the contrary, Eq. (5) adapted by the FSC model yields a weaker dependence of intermediately steady turbulent burning velocity on the rms turbulent velocity, i.e. $U_{t,ISP} \propto u'^{0.75}$. The point is that, as shown by Verma and Lipatnikov (2016), transient, curvature and strain effects can significantly change the scaling exponent for simulated turbulent flame speed as a function of the rms turbulent velocity.

Fig. 9 shows that the simulations (see lines) reasonably well predict a slow increase in the mean flame speed with the mean flame radius at various u', while the effect magnitude is underestimated at $u' = 3.31$ m/s, especially at smaller $\overline{R}_f$.

5. Concluding remarks

The Flame Speed Closure (FSC) model of the influence of turbulence on premixed combustion was implemented into the open source platform OpenFOAM. The implementation of the FSC model was numerically verified using benchmark analytical solutions in the cases of statistically 1-D planar and spherical turbulent flames. The FSC model supplemented with the well-known $k - \varepsilon$ model of turbulence was applied to unsteady 3-D RANS simulations of small-scale laboratory dust-explosion experiments performed under well-controlled conditions using the Leeds fan-stirred combustion vessel. Numerical results show that the model well predicts (i) an increase in the apparent turbulent

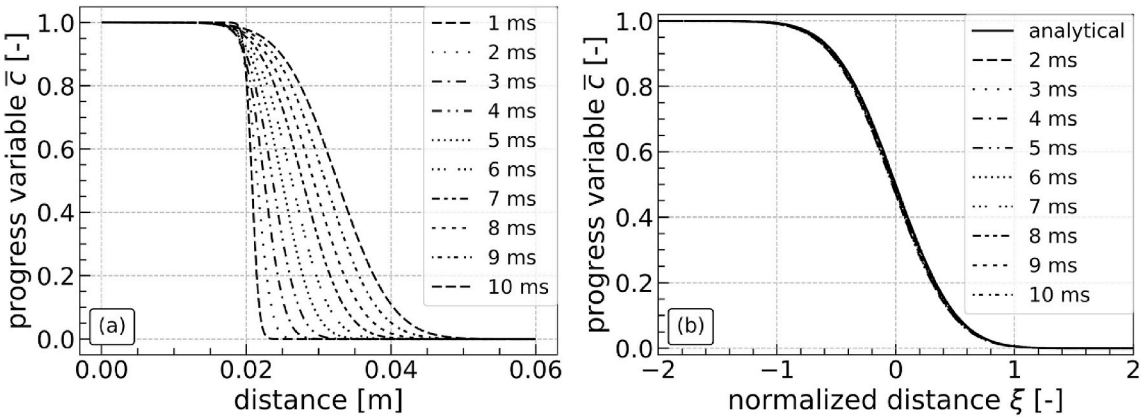

Fig. 5. Spatial profiles of the Reynolds-averaged combustion progress variable obtained from statistically1-D spherical flame propagating in "frozen" turbulence. (a) Reynolds-averaged combustion progress variable $\bar{c}$ vs. distance x, (b) $\bar{c}$ vs. the normalized distance ξ defined by Eq. (9).

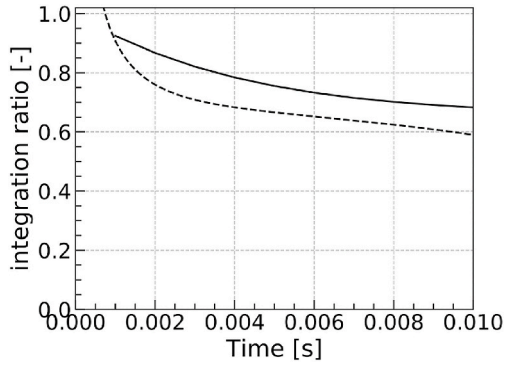

Fig. 6. Comparison of ratios of $\int_0^\infty \tilde{c}\bar{r}dr \left\{ \int_0^\infty \bar{c}\bar{r}dr \right\}^{-1}$, solid line, and $S_{t,b}/(\sigma U_t)$, dashed line, computed for expanding statistically 1-D spherical flame.

flame speed by the rms turbulent velocity at moderate turbulence and (ii) a slow increase in the flame speed with growth of the mean flame radius.

Thus, the present work indicates that the FSC model could be an

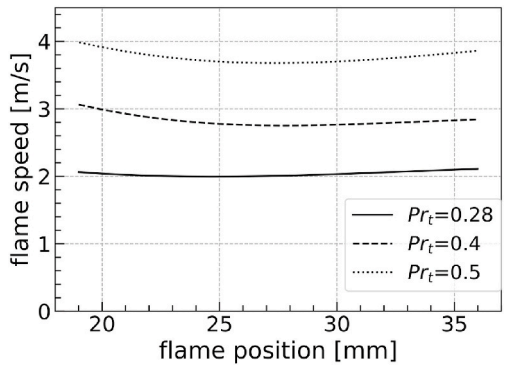

Fig. 7. Mean flame speeds computed for different turbulent Prandtl numbers specified in legends vs. mean flame position. $u' = 3.31$ m/s.

appropriate building block for developing an advanced numerical tool for CFD research into large-scale explosions of fine dust particles with high volatile contents. For this purpose, models of other phenomena (e.g. Darrieus-Landau and Rayleigh-Taylor instabilities of initially laminar flame kernel, acceleration of large-scale flames attributed commonly to flame-generated turbulence, radiative heat transfer, etc.) should be

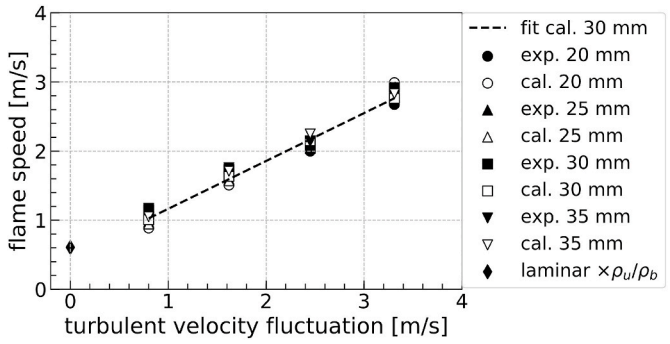

Fig. 8. Comparison of computed (open symbols) and measured (filled symbols) mean flame speeds. The diamond symbol represents the laminar flame speed multiplied with the density ratio. The dashed line shows a linear fit to the flame-speed data computed at a mean flame radius of 30 mm.

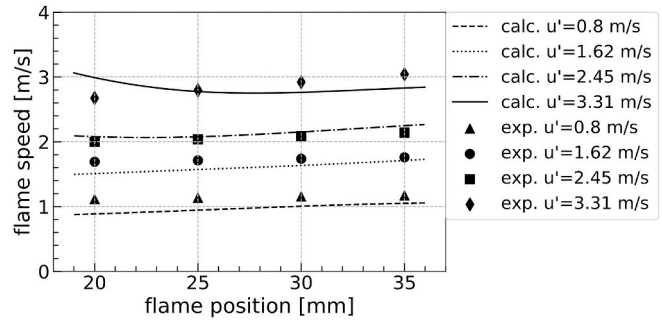

Fig. 9. Computed (lines) and measured (symbols) mean flame speeds vs. mean flame position.

invoked, combined with the FSC model and implemented into OpenFOAM. This is the goal for our future work.

Credit author statement

Chen Huang: Conceptualization, Software, Validation, Writing - original draft, Writing - review & editing, Visualization, Project administration, Funding acquisition. Andrei Lipatnikov: Conceptualization, Methodology, Validation, Writing - original draft, Writing - review & editing, Supervision, Funding acquisition. Ken Nessvi: Conceptualization, Writing - original draft, Writing - review & editing.

Declaration of competing interest

The authors declare that they have no known competing financial interests or personal relationships that could have appeared to influence the work reported in this paper.

Acknowledgements

The authors would like to acknowledge AFA-Försäkring for financial support of this project (grant number 180028).

Appendix A. Supplementary data

Supplementary data to this article can be found online at https://doi.org/10.1016/j.jlp.2020.104237.

References

Abdel-Gayed, R.G., Al-Khishali, K.J., Bradley, D., 1984. Turbulent burning velocities and flame straining in explosions. Proc. Roy. Soc. Lond. A 391 (1801), 393–414. https://doi.org/10.1098/rspa.1984.0019.

Ansys. Cfx. https://www.ansys.com/products/fluids/ansys-cfx. (Accessed 23 April 2020).

Ansys. Fluent. https://www.ansys.com/products/fluids/ansys-fluent. (Accessed 23 April 2020).

The Leader in Powertrain CFD AVL. Fire. https://www.avl.com/sv/fire. (Accessed 23 April 2020).

Bauwens, C.R., Chaffee, J.L., Dorofeev, S., 2008. Experimental and numerical study of methane-air deflagrations in a vented enclosure. Fire Saf. Sci. 9, 1043–1054. https://doi.org/10.3801/IAFSS.FSS.9-1043.

Bauwens, C.R., Chaffee, J.L., Dorofeev, S.B., 2011. Vented explosion overpressures from combustion of hydrogen and hydrocarbon mixtures. Int. J. Hydrogen Energy 36 (3), 2329–2336. https://doi.org/10.1016/j.ijhydene.2010.04.005.

Beck, H., Jeske, A., 1982. Dokumentation Staubexplosionen: Analyse und Einzelfalldarstellung. Berufsgenossenschaftliches Institut für Arbeitssicherheit, vol. 3. Arbeitsstoffe Staubtechnik, Fachbereich.

Bradley, D., Habik, S.E.D., Swithenbank, J.R., 1988. Laminar burning velocities of CH4—air-graphite mixtures and coal dusts. Proc. Combust. Inst. 21 (1), 249–256. https://doi.org/10.1016/S0082-0784(88)80252-2.

Bradley, D., Chen, Z., Swithenbank, J.R., 1989a. Burning rates in turbulent fine dust-air explosions. Proc. Combust. Inst. 22 (1), 1767–1775.

Bradley, D., Dixon-Lewis, G., Habik, S.E.D., 1989b. Lean flammability limits and laminar burning velocities of CH4-air-graphite mixtures and fine coal dusts. Combust. Flame 77 (1), 41–50. https://doi.org/10.1016/0010-2180(89)90103-X.

Bradley, D., Haq, M.Z., Hicks, R.A., Kitagawa, T., Lawes, M., Sheppard, C.G.W., Woolley, R., 2003. Turbulent burning velocity, burned gas distribution, and associated flame surface definition. Combust. Flame 133 (4), 415–430. https://doi.org/10.1016/S0010-2180(03)00039-7.

Bray, K.N.C., Moss, J.B., 1977. A unified statistical model of the premixed turbulent flame. Acta Astronaut. 4, 291–319. https://doi.org/10.1016/0094-5765(77)90053-4.

Cloney, C.T., Ripley, R.C., Pegg, M.J., Amyotte, P.R., 2018. Laminar burning velocity and structure of coal dust flames using a unity Lewis number CFD model. Combust. Flame 190, 87–102. https://doi.org/10.1016/j.combustflame.2017.11.010.

Converge. CFD, software. https://convergecfd.com/. (Accessed 23 April 2020).

Demir, S., Bychkov, V., Chalagalla, S.H.R., Akkerman, V.y., 2017. Towards a predictive scenario of a burning accident in a mining passage. Combust. Theor. Model. 21 (6), 997–1022. https://doi.org/10.1080/13647830.2017.1328129.

Demir, S., Calavay, A.R., Akkerman, V.y., 2018. Influence of gas compressibility on a burning accident in a mining passage. Combust. Theor. Model. 22 (2), 338–358. https://doi.org/10.1080/13647830.2017.1403654.

Driscoll, J., 2008. Turbulent premixed combustion: flamelet structure and its effect on turbulent burning velocities. Prog. Energy Combust. Sci. 34, 91–134.

En14491, 2012. Dust Explosion Venting Protective Systems.

FINE, 2019. FINE/Marine. The Leading CFD Software for Naval Architects and Marine Engineers. https://www.numeca.com/en_eu/product/finemarine. (Accessed 23 April 2020).

Gant, S., Hoyes, J., 2010. Review of FLACS Version 9.0 Dispersion Modelling Capabilities. Health and Safety Executive HSE Books.

Ghaffari, M., Hoffmann, A.C., Skjold, T., Eckhoff, R.K., van Wingerden, K., 2019. A brief review on the effect of particle size on the laminar burning velocity of flammable dust: application in a large-scale CFD tool. J. Loss Prevent. Proc. 103929 https://doi.org/10.1016/j.jlp.2019.103929.

Han, D., Satija, A., Gore, J.P., Lucht, R.P., 2018. Experimental study of CO_2 diluted, piloted, turbulent CH4/air premixed flames using high-repetition-rate OH PLIF. Combust. Flame 193, 145–156.

Hinze, J.O., 1975. Turbulence, second ed. McGraw-Hill, New York.

Huang, C., Yasari, E., Johansen, L.C.R., Hemdal, S., Lipatnikov, A.N., 2016. Application of flame speed closure model to RANS simulations of stratified turbulent combustion in a gasoline direct-injection spark-ignition engine. Combust. Sci. Technol. 188, 98–131. https://doi.org/10.1080/00102202.2015.1083988.

Karlovitz, B., Denniston, D.W., Wells, F.E., 1951. Investigation of turbulent flames. J. Chem. Phys. 19, 541–547.

Karpov, V.P., Semenov, E.S., Sokolik, A.S., 1959. Turbulent combustion in an enclosed space. Proc. Acad. Sci. USSR. Phys. Chem. Sec. 128, 871–873.

Karpov, V.P., Lipatnikov, A.N., Zimont, V.L., 1996. A test of an engineering model of premixed turbulent combustion. Proc. Combust. Inst. 26, 249–257.

Launder, B.E., Spalding, D.B., 1972. Mathematical Models of Turbulence. Academic Press, London.

Libby, P.A., Bray, K.N.C., 1977. Variable density effects in premixed turbulent flames. AIAA J. 15, 1186–1193. https://doi.org/10.2514/3.60770.

Liberman, M.A., Ivanov, M.F., Kiverin, A.D., 2015. Effects of thermal radiation heat transfer on flame acceleration and transition to detonation in particle-cloud hydrogen flames. J. Loss Prevent. Proc. 38, 176–186. https://doi.org/10.1016/j.jlp.2015.09.006.

Lipatnikov, A.N., 2009. Testing premixed turbulent combustion models by studying flame dynamics. Int. J. Spray and Combust. 1 (1), 39–66. https://doi.org/10.1260/175682709788083362.

Lipatnikov, A., 2012. Fundamentals of Premixed Turbulent Combustion. CRC Press.

Lipatnikov, A.N., 2018. RANS simulations of premixed turbulent flames. In: De, S., Agarwal, A.K., Chaudhuri, S., Sen, S. (Eds.), Modeling and Simulation of Turbulent Combustion. Springer Nature Singapore Pte Ltd., Singapore, pp. 181–240.

Lipatnikov, A.N., Chomiak, J., 1997. A simple model of unsteady turbulent flame propagation. SAE Trans. Sect. 3, J. Engines 106, 2441–2452.

Lipatnikov, A.N., Chomiak, J., 2002a. Turbulent flame speed and thickness: phenomenology, evaluation, and application in multi-dimensional simulations. Prog. Energ. Combust. 28 (1), 1–74. https://doi.org/10.1016/S0360-1285(01)00007-7.

Lipatnikov, A.N., Chomiak, J., 2002b. Turbulent burning velocity and speed of developing, curved, and strained flames. Proc. Combust. Inst. 29 (2), 2113–2121.

Lipatnikov, A.N., Chomiak, J., 2005a. A theoretical study of premixed turbulent flame development. Proc. Combust. Inst. 30, 843–850.

Lipatnikov, A.N., Chomiak, J., 2005b. Self-similarly developing, premixed, turbulent flames: a theoretical study. Phys. Fluids 17, 065105.

Lipatnikov, A.N., Chomiak, J., 2005c. Molecular transport effects on turbulent flame propagation and structure. Prog. Energy Combust. Sci. 31 (1), 1–73. https://doi.org/10.1016/j.pecs.2004.07.001.

Lipatnikov, A.N., Chomiak, J., 2007. Global stretch effects in premixed turbulent combustion. Proc. Combust. Inst. 31, 1361–1368.

Nfp, A.68, 2018. Standard on Explosion Protection by Deflagration Venting. National Fire Protection Association, Quincy, MA, USA.

Open, F.O.A.M., 2019. The Open Source CFD Toolbox. http://openfoam.com. (Accessed 23 April 2020).

Prudnikov, A.G., 1967. Burning of homogeneous fuel-air mixtures in a turbulent flow. In: Raushenbakh, B.V. (Ed.), Physical Principles of the Working Process in Combustion Chambers of Jet Engines. Clearing House for Federal Scientific & Technical Information, Springfield, Ohio, pp. 244–336.

Sezer, H., Kronz, F., Akkerman, V.y., Rangwala, A.S., 2017. Methane-induced explosions in vented enclosures. J. Loss Prevent. Proc. 48, 199–206. https://doi.org/10.1016/j.jlp.2017.04.009.

Shimura, K., Matsuo, A., 2019. Using an extended CFD–DEM for the two-dimensional simulation of shock-induced layered coal-dust combustion in a narrow channel. Proc. Combust. Inst. 37 (3), 3677–3684. https://doi.org/10.1016/j.proci.2018.07.066.

Sinha, A., Rao, V.C.M., Wen, J.X., 2019. Modular phenomenological model for vented explosions and its validation with experimental and computational results. J. Loss Prevent. Proc. 61, 8–23. https://doi.org/10.1016/j.jlp.2019.05.017.

Skjold, T., 2003. Selected Aspects of Turbulence and Combustion in 20-litre Explosion Vessels: Development of Experimental Apparatus and Experimental Investigation. Master's thesis. The University of Bergen.

Skjold, T., 2007. Review of the DESC project. J. Loss Prevent. Proc. 20 (4–6), 291–302. https://doi.org/10.1016/j.jlp.2007.04.017.

Skjold, T., 2014. Flame Propagation in Dust Clouds. Numerical Simulation and Experimental Investigation. Phd thesis. The University of Bergen.

Skjold, T., Arntzen, B.J., Hansen, O.R., Taraldset, O.J., Storvik, I.E., Eckhoff, R.K., 2005. Simulating dust explosions with the first version of DESC. Process Saf. Environ. 83 (2), 151–160. https://doi.org/10.1205/psep.04237.

Skjold, T., Arntzen, B.J., Hansen, O.R., Storvik, I.E., Eckhoff, R.K., 2006. Simulation of dust explosions in complex geometries with experimental input from standardized tests. J. Loss Prevent. Proc. 19 (2–3), 210–217. https://doi.org/10.1016/j.jlp.2005.06.005.

Skjold, T., Hisken, H., Lakshmipathy, S., Atanga, G., Carcassi, M., Schiavetti, M., Stewart, J.R., Newton, A., Hoyes, J.R., Tolias, I.C., Venetsanos, A.G., Hansen, O.R., Geng, J., Huser, A., Helland, S., Jambut, R., Ren, K., Kotchourko, A., Jordan, T., Daubech, J., Lecocq, G., Hanssen, A.G., Kumar, C., Krumenacker, L., Jallais, S., Miller, D., Bauwens, C.R., 2019a. Blind-prediction: estimating the consequences of vented hydrogen deflagrations for homogeneous mixtures in 20-foot ISO containers. Int. J. Hydrogen Energy 44 (17), 8997–9008. https://doi.org/10.1016/j.ijhydene.2018.06.191.

Skjold, T., Hisken, H., Bernard, L., Mauri, L., Atanga, G., Lakshmipathy, S., Lucas, M., Carcassi, M., Schiavetti, M., Chandra Madhav Rao, V., Sinha, A., Wen, J.X., Tolias, I.C., Giannissi, S.G., Venetsanos, A.G., Stewart, J.R., Hansen, O.R., Kumar, C., Krumenacker, L., Laviron, F., Jambut, R., Huser, A., 2019b. J. Loss Prevent. Proc. 61, 220–236. https://doi.org/10.1016/j.jlp.2019.06.013.

Song, Y., Zhang, Q., 2019. Multiple explosions induced by the deposited dust layer in enclosed pipeline. J. Hazard Mater. 371, 423–432. https://doi.org/10.1016/j.jhazmat.2019.03.040.

Song, Y., Zhang, Q., Wu, W., 2017. Interaction between gas explosion flame and deposited dust. Process Saf. Environ. 111, 775–784. https://doi.org/10.1016/j.psep.2017.09.004.
Spijker, C., Kern, H., Held, K., Raupenstrauch, H., 2013. Modelling Dust Explsions. AIChE annual meeting 2013, San Francisco, United States.
Sponfeldner, T., Soulopoulos, N., Beyrau, F., Hardalupas, Y., Taylor, A.M.K.P., Vassilicos, J.C., 2015. The structure of turbulent flames in fractal- and regular-grid-generated turbulence. Combust. Flame 162, 3379–3393.
Tamadonfar, P., Gülder, Ö.L., 2014. Flame brush characteristics and burning velocities of premixed turbulent methane/air Bunsen flames. Combust. Flame 161, 3154–3165.
Tascón, A., Aguado, P.J., 2015. CFD simulations to study parameters affecting dust explosion venting in silos. Powder Technol. 272, 132–141. https://doi.org/10.1016/j.powtec.2014.11.031.
Tascón, A., Aguado, P.J., 2017. Simulations of vented dust explosions in a 5 m3 vessel. Powder Technol. 321, 409–418. https://doi.org/10.1016/j.powtec.2017.08.047.
Taylor, G.I., 1935. Statistical theory of turbulence. IV. Diffusion in a turbulent air stream. Proc. Roy. Soc. Lond. A 151, 65–78.
Tolias, I.C., Stewart, J.R., Newton, A., Keenan, J., Makarov, D., Hoyes, J.R., et al., 2018. Numerical simulations of vented hydrogen deflagration in a medium-scale enclosure. J. Loss Prevent. Proc. 52, 125–139. https://doi.org/10.1016/j.jlp.2017.10.014.
Ugarte, O.J., Akkerman, V.y., Rangwala, A.S., 2016. A computatinal platform for gas explosion venting. Process Saf. Environ. 99, 167–174. https://doi.org/10.1016/j.psep.2015.11.001.
Vdi3673, 2002. Pressure release of dust explosions. Guideline VDI 3673 Part 1.
Vendra, C.M.R., Wen, J.X., 2019. Numerical modelling of vented lean hydrogen deflagations in an ISO container. Int. J. Hydrogen Energy 44 (17), 8767–8779. https://doi.org/10.1016/j.ijhydene.2018.11.093.
Verma, S., Lipatnikov, A.N., 2016. Does sensitivity of measured scaling exponents for turbulent burning velocity to flame configuration prove lack of generality of notion of turbulent burning velocity? Combust. Flame 173 (1), 77–88. https://doi.org/10.1016/j.combustflame.2016.08.018.
Vyazmina, E., Jallais, S., Krumenacker, L., Tripathi, A., Mahon, A., Commanay, J., et al., 2019. Vented explosion of hydrogen/air mixture: an intercomparison benchmark exercise. Int. J. Hydrogen Energy 44 (17), 8914–8926. https://doi.org/10.1016/j.ijhydene.2018.07.195.
Weller, H.G., Tabor, G., Gosman, A.D., Fureby, C., 1998. Application of a flame-wrinkling LES combustion model to a turbulent mixing layer. Proc. Combust. Inst. 27 (1), 899–907. https://doi.org/10.1016/S0082-0784(98)80487-6.
Yasari, E., Verma, S., Lipatnikov, A.N., 2015. RANS simulations of statistically stationary premixed turbulent combustion using Flame Speed Closure model. Flow, Turbul. Combust. 94, 381–414. https://doi.org/10.1007/s10494-014-9585-x.
Zimont, V.L., 1979. Theory of turbulent combustion of a homogeneous fuel mixture at high Reynolds number. Combust. Explos. Shock Waves 15, 305–311.
Zimont, V.L., 2000. Gas premixed combustion at high turbulence. Turbulent flame closure combustion model. Exp. Therm. Fluid Sci. 21, 179–186. https://doi.org/10.1016/S0894-1777(99)00069-2.
Zimont, V.L., Lipatnikov, A.N., 1993. To computations of the heat release rate in turbulent flames. Dokl. Phys. Chem. 332, 592–594.
Zimont, V.L., Lipatnikov, A.N., 1995. A numerical model of premixed turbulent combustion of gases. Chem. Phys. Reports 14 (7), 993–1025.